SRSF2 is a key player in orchestrating the directional migration and differentiation of MyoD progenitors during skeletal muscle development

Rula Sha[1#], Ruochen Guo[1#], Huimin Duan[2], Qian Peng[1], Ningyang Yuan[1], Zhenzhen Wang[1], Zhigang Li[1], Zhiqin Xie[1], Xue You[2*] and Ying Feng[1,2*]

[1]CAS Key Laboratory of Nutrition, Metabolism and Food Safety, Shanghai Institute of Nutrition and Health, University of Chinese Academy of Sciences, Chinese Academy of Sciences, China. [2] Lin He's Academician Workstation of New Medicine and Clinical Translation in Jining Medical University, Jining Medical University, Jining, China.

Co-first authors

*Correspondence: Xue You, youxue19910@163.com (email);

Ying Feng, fengying@sinh.ac.cn (email) (Lead Contact)

Abstract

SRSF2 plays a dual role, functioning both as a transcriptional regulator and a key player in alternative splicing. The absence of SRSF2 in MyoD+ progenitors resulted in perinatal mortality in mice, accompanied by severe skeletal muscle defects. SRSF2 deficiency disrupts the directional migration of MyoD progenitors, causing them to disperse into both muscle and non-muscle regions. Single-cell RNA-sequencing analysis revealed significant alterations in SRSF2-deficient myoblasts, including a reduction in extracellular matrix components, diminished expression of genes involved in ameboid-type cell migration and cytoskeleton organization, mitosis irregularities, and premature differentiation. Notably, one of the targets regulated by SRSF2 is the serine/threonine kinase Aurka. Knockdown of Aurka led to reduced cell proliferation, disrupted cytoskeleton, and impaired differentiation, reflecting the effects seen with SRSF2 knockdown. Crucially, the introduction of exogenous Aurka in SRSF2-knockdown cells markedly alleviated the differentiation defects caused by SRSF2 knockdown. Furthermore, our research unveiled the role of SRSF2 in controlling alternative splicing within genes associated with human skeletal muscle diseases, such as BIN1, DMPK, FHL1, and LDB3. Specifically, the precise knockdown of the Bin1 exon17-containing variant, which is excluded following SRSF2 depletion, profoundly disrupted C2C12 cell differentiation. In summary, our study offers valuable insights into the role of SRSF2 in governing MyoD progenitors to specific muscle regions, thereby controlling their differentiation through the regulation of targeted genes and alternative splicing during skeletal muscle development.

Introduction

Myogenic progenitors (MPCs) are a specialized type of precursor cell responsible for the formation of skeletal muscle cells during embryonic development. The process begins with the transformation of the dermomyotome into segmented structures known as somites, which serve as a reservoir for MPCs expressing essential transcription factors Pax3 and Pax7(Relaix et al., 2006; Relaix et al., 2005). These MPCs acquires their myogenic identity by activating specific myogenic regulatory factors, including Myf5, MyoD, Myog and Myf6(Braun and Gautel, 2011).

Among these factors, Myf5+ progenitors are key players in expanding the myogenic progenitor pool through extensive proliferation, as well as in the initial migration from somites to muscle-forming regions and the establishment of early muscle primordia(Tajbakhsh et al., 1996). The absence of Pax3 and Myf5 results in the inactivation of MyoD, ultimately leading to the absence of skeletal muscles in the body(Tajbakhsh et al., 1997). This highlights the hierarchical relationship between Myf5 and MyoD, with Myf5 acting as an upstream regulator of MyoD. Myf5+ progenitors serve as a source for MyoD+ progenitors, these two populations collaborate in a coordinated manner to ensure the proper formation and growth of skeletal muscles during embryonic development(Rodriguez-Outeirino et al., 2021). In the perinatal stages, MPCs play a crucial role in establishing the satellite cell (SC) pool, which serve as a reservoir of muscle stem cells(Relaix *et al.*, 2005). MyoD was not expressed in quiescent SCs but showed high levels of expression in activated and proliferative myoblasts, which are the progeny of SCs (Zammit et al., 2004).

The extracellular matrix (ECM) and cytoskeleton play vital roles in maintaining the structural integrity of cells and tissues, while also exerting a profound influence on cell behavior(Csapo et al., 2020; D'Urso and Kurniawan, 2020). Specifically, the ECM serves as a scaffold for cell adhesion and migration, playing a critical role in regulating signaling pathways that control cell proliferation, differentiation, and survival(Csapo *et al.*, 2020). On the other hand, the cytoskeleton is responsible for maintaining cell shape and polarity, facilitating intracellular transport, and aiding in cell division(D'Urso and

Kurniawan, 2020). In the context of skeletal muscle development, interactions of MPCs with the ECM, as well as the dynamic rearrangements of the cytoskeleton, are critical for guiding directional migration of MPCs (Choi et al., 2020; Yin et al., 2013). Actin filaments, a fundamental component of the cytoskeleton, undergo dynamic changes leading to the formation of protrusions like lamellipodia and filopodia, which assist in forward movement(Lappalainen et al., 2022). Meanwhile, microtubules, another critical part of the cytoskeleton, contribute to cell polarity and play a role in establishing and maintaining direction during migration. The reduction of both ECM and cytoskeleton components has a significant impact on myoblast migration, cell division and differentiation(Osses et al., 2009; Zhang et al., 2021).

It's noteworthy that splicing and transcription regulator SRSF2 emerges as a critical regulator that inhibits apoptosis in My5+progenitors and maintain their migratory capability during embryonic skeletal muscle development. The absence of SRSF2 in Myf5+ progenitors leads to a high rate of myoblasts apoptosis, as well as aberrant migration, ultimately resulting in the complete loss of mature myofibers(Guo et al., 2022). This emphasizes the essential role of SRSF2 in promoting the survival of Myf5+ progenitors and its significance in ensuring the successful progression of skeletal muscle development.

In this study, we observed that the absence of SRSF2 in MyoD+ progenitors resulted in the perinatal mortality in mice, primarily due to respiratory failure. SRSF2 deficiency markedly disrupted the directional migration capacity of MyoD+ progenitors, causing them to disperse into both muscle and non-muscle regions. Single-cell RNA-sequencing (scRNA-seq) analysis revealed notable changes in SRSF2-deficient myoblasts, including reduced ECM components, diminished expression of genes involved in ameboid-type cell migration and cytoskeleton organization, mitosis irregularities, and impaired differentiation. Significantly, SRSF2 regulates the expression of the serine/threonine kinase Aurka. Knockdown of Aurka resulted in decreased cell proliferation and impaired differentiation, resembling SRSF2 knockdown effects. Aurka overexpression in SRSF2-depleted cells significantly

rescued the differentiation defects, underscoring the critical role of SRSF2-regulated Aurka expression in myoblast differentiation. Furthermore, our findings demonstrated the involvement of SRSF2 in alternative splicing of genes linked to human skeletal muscle diseases, including BIN1, DMPK, FHL1, and LDB3. Specifically, targeted knockdown of the Bin1 exon17-containing variant, skipped upon SRSF2 depletion, severely disrupted myoblast differentiation. In summary, our study provides valuable insights into SRSF2's role in directing MyoD progenitors to distinct muscle regions, thereby regulating their differentiation through targeted gene regulation and alternative splicing during skeletal muscle development.

Results

Inactivation of SRSF2 in MyoD+ progenitors led to significant differentiation defects in skeletal muscle, resulting in perinatal death in mice

The absence of SRSF2 in Myf5+ progenitors results in a significant increase in myoblasts apoptosis during embryonic development. This genetic condition leads to rib deformities and muscle loss in the limbs and body wall in mice, causing the demise of knockout pups immediately after birth(Guo *et al.*, 2022). To eliminate the potential influence of rib deformities on mouse mortality and to concentrate on SRSF2's role on myogenesis, we employed a selective disruption of the *Srsf2* gene in MyoD+ myogenic progenitors through crossbreeding SRSF2$^{f/f}$ mice (WT) with MyoD^{Cre} mice (Chen et al., 2005), leading to the generation of SRSF2$^{f/f}$;Myod-cre mice (SRSF2-KO) (Fig.S1).

Newborn KO pups exhibited normal morphology but had empty stomachs without any milk and showed reduced body weight compared to their WT counterparts (Fig.1A and 1B). KO pups did not survive beyond the second day after birth (Fig.1C), suggesting potential respiratory issues. This observation prompted us to examine the condition of their lungs. The lungs of KO pups appeared congested compared to those of WT pups, and they sank in water while WT lungs floated (Fig. 1D). HE staining further revealed collapsed alveoli in the KO lungs at postnatal day 1 (P1) (Fig.1E).

Histological examination of various skeletal muscles regions revealed striking

differentiation defects in P1 KO mice. Notably, the characteristic myofibers typically observed in the longitudinal sections of WT controls were conspicuously absent, instead replaced by shortened, irregular fibers in KO mice (Fig. 1F, top panel). These muscle abnormalities were consistently observed in the tongue and diaphragm as well (Fig. 1F, bottom panel). In transverse sections of the diaphragm from KO mice, there was a noticeable reduction in diaphragm thickness and the presence of cavities within the muscle fibers (Fig. 1G). Desmin, a marker for myoblasts and newly formed fibers, exhibited significantly weaker staining in hindlimb sections of the KO group compared to the control group (Fig. 1H). Myh3, a marker for terminal differentiation, displayed an irregular and loosened staining pattern along with the presence of central nuclei features in intercostal muscle sections of the KO group (Fig. 1I). In summary, the deficiency of SRSF2 had a profound and disruptive impact on the formation of skeletal muscles, resulting in dysfunction that rendered KO mice unable to suckle for milk and breathe effectively.

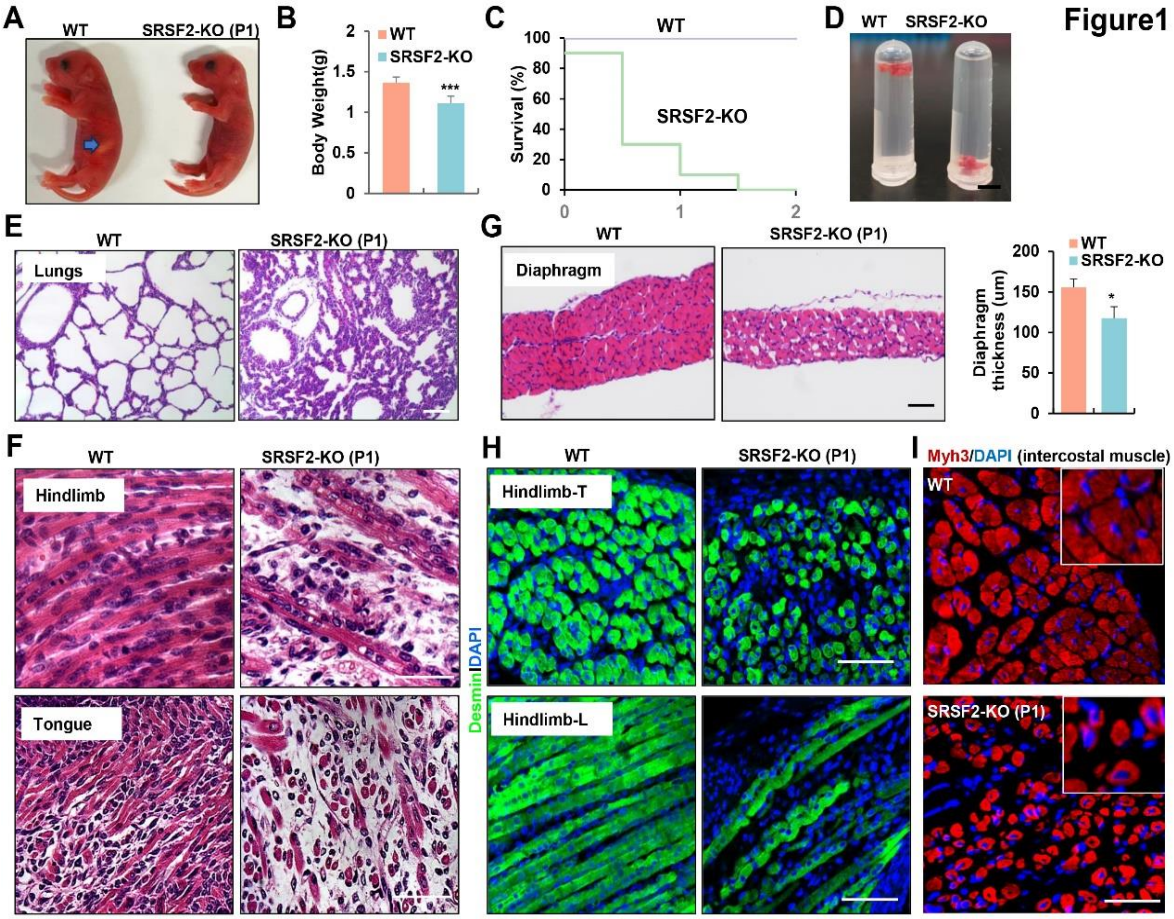

Figure 1. Inactivation of SRSF2 in MyoD+ progenitors resulted in skeletal muscle dysfunction and respiratory failure. (A) Macroscopic appearance of WT and SRSF2-KO pups immediately after birth (P1). Scale bars, 5 mm. (B) Comparison of body weight between WT and SRSF2-KO pups (n=10). (C) Survival curve of WT and SRSF2-KO pups (n=10). (D) Sinking test for lungs excised from P1 WT and SRSF2-KO mice and placed in a 5 ml Ep tube. (E) Representative HE staining of lung sections at P1 (n=3). Scale bars, 50 μm. (F) Representative HE staining on longitudinal sections of hindlimbs (top panels), and transverse tongue sections at P1 (bottom panels) (n=3). Scale bars, 10 μm. (G) Representative HE staining of transverse-sections of diaphragms at P1 (n=3). Scale bars, 50 μm. Comparison of diaphragm thickness is displayed on the right. (H) Representative confocal images of desmin staining in transverse-sections and longitudinal sections of hindlimbs from WT and SRSF2-KO at P1 (n=3). Scale bars, 10 μm. (I) Representative confocal images of Myh3 staining in intercostal muscle sections of WT and SRSF2-KO at P1 (n=3). Scale bars, 10 μm. Enlarged views shown on the upper right corners.

RNA-seq analysis and disrupted sarcomere structures in KO skeletal muscle

To explore the molecular mechanisms underlying SRSF2 deficiency in skeletal muscle differentiation, we conducted RNA-seq analysis on diaphragm muscle samples collected from P1 mice. Differential gene analysis identified 160 up-regulated genes and 244 down-regulated genes (Fig. 2A). Gene Ontology (GO) analysis showed that these differentially expressed genes (DEGs) were significantly enriched in key cellular components, including mitochondria, myosin complex, contractile fibers, Z-disc, among others. Moreover, these DEGs displayed enrichment crucial molecular functions such as transmembrane transporter activity, integrin binding, cytoskeletal protein binding, among others (Fig. 2B).

To validate these findings, we selected several genes based on their functions. For example, Scn4b encodes a protein associated with voltage-gated sodium channels, while Stac2 is involved in the regulation of calcium ion influx in muscle cells. Symm plays a key role in the formation of sarcomeres, which are the contractile unites of muscle cells, and Tmod4 is responsible for maintaining the structural integrity of skeletal muscle by regulating the stability of actin filaments. Our qPCR analysis provided further confirmation by demonstrating a significant reduction in the expression levels of these selected genes in the KO group (Fig. 2C).

Actin is a major component of the thin filaments in the sarcomeres, and phalloidin is a fluorescent compound that selectively binds to and labels F-actin (filamentous actin). Phalloidin labeling in diaphragm sections revealed disarrangement of actin filaments in the KO group when compared to the WT group (Fig. 2D). To gain deeper insights, we conducted transmission electron microscopy experiments to examine the sarcomere and Triad structures in the hindlimb sections. Sarcomeres are characterized by their highly organized structure, while Triads are specialized structures involved in the regulation of calcium ions required for muscle contraction. Our findings revealed well-organized sarcomere and Triad structures in the WT group. In contrast, these structures were substantially disrupted in the KO group (Fig. 2E). This disruption could lead to impaired muscle functions, affecting their ability to contract ad relax efficiently.

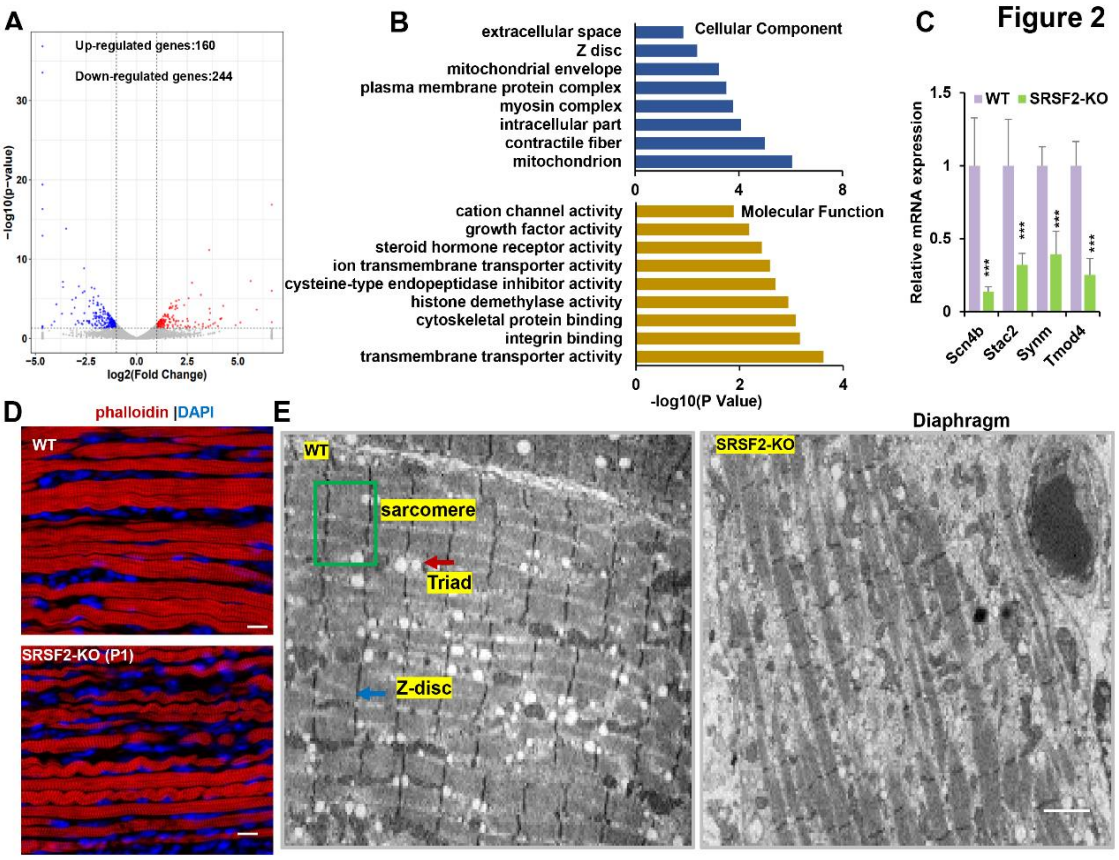

Figure 2. RNA-seq analysis and disrupted sarcomere structures in the KO skeletal muscle. (A) RNAs-seq was conducted on P1 diaphragm samples. Based on statistical significance (P value <0.05) and fold change, over 160 upregulated genes and 244 downregulated genes were identified. (B) Gene Ontology (GO) enrichment analysis of

differentially expressed genes (DEGs) was performed, focusing on their cellular component and molecular function categories. (C) qPCR analysis on a selection of genes based on RNA-seq data, using P1 diaphragm samples (n=6). (D) Representative confocal images of phalloidin staining in longitudinal sections of P1 diaphragm muscle of WT and SRSF2-KO mice. Scale bars, 10 μm. (E) Transmission electron microscopy images of the diaphragm in newborn WT and SRSF2-KO mice. Sarcomere is indicated by the green box, Z-disc by the blue arrow, and Triad by the red arrow. Scale bars, 20 μm.

SRSF2 deficiency impairs the directional migration of MyoD+ progenitors and their subsequent differentiation during skeletal muscle development

We then developed a tracer mouse model through the crossbreeding of Rosa26-tdTomato mice with MyoD^{cre} and SRSF2$^{f/f}$ mice (Fig. 3A). This approach allowed us to monitor and track the destiny of MyoD-derived cells, those that had previously exhibited MyoD expression or were currently expressing MyoD throughout the critical phases of skeletal muscle development.

In the analysis of embryo sections harvested from control mice at E14.5, the utilization of tdT staining, MHC staining, and the subsequent examination of the co-localization of tdT and MHC signals provided unequivocal evidence of the successful migration of MyoD-derived cells into the muscle region (Fig. 3B, 3C and Fig. S2). Subsequently, these cells underwent proliferation and differentiation, ultimately culminating in their significant contributions to the development of a highly organized muscle structure. In tdT/KO sections, MyoD-derived cells not only migrated into the intended muscle region but also dispersed widely into numerous non-muscular territories (Fig. 3B, white arrows). This intriguing pattern strongly suggests migration defects of MyoD-derived cells resulting from the loss of SRSF2 at this stage. Moreover, even within the confines of the muscle region, tdT/KO embryos displayed a marked reduction in the degree of cellular differentiation when compared to the control (Fig. 3C). This impaired differentiation ultimately led to noticeable lack of precise co-localization between tdT and MHC signals (Fig. S2).

Consistent with the migratory defects observed in E14.5 KO sections, in the hindlimb sections of E15.5 KO mice, as well as the hindlimb and intercostal muscle

sections of KO mice at the perinatal stage (P1), tdT staining also revealed a substantial presence of MyoD-derived cells distributed beyond the muscle regions (Fig. 3D-3F, white arrows). These findings further confirmed that the deficiency in SRSF2 profoundly impacts the capacity of MyoD-derived cells to undergo directed migration specifically into the skeletal muscle region.

Moreover, we conducted immunostaining on both longitudinal and cross-sections of diaphragm in newborn mice (P1). In the control group, our examination of longitudinal sections revealed a remarkable co-localization between the tdT signals and the densely compacted muscle fibers stained with MHC (Fig. 3G). Within the cross-sectional views, the tdT-stained regions exhibited a consistent and well-organized arrangement, surrounded by laminin (Fig. 3H). In contrast, the KO mice exhibited noticeable gaps between muscle fibers in the longitudinal sections of diaphragm, with only tdT signals present within these loosely arranged fibers (Fig. 3G, white arrows). Furthermore, the tdT-stained areas appeared disorganized within the cross-sectional views, characterized by numerous cavities within them (Fig. 3H, white arrows). The presence of similar cavities was also observed in the hindlimb sections of P1 KO mice (Fig. 3I, white arrows). These collective observations underscore the critical role of SRSF2 in regulating both the migration and differentiation processes of MyoD-derived cells during muscle development.

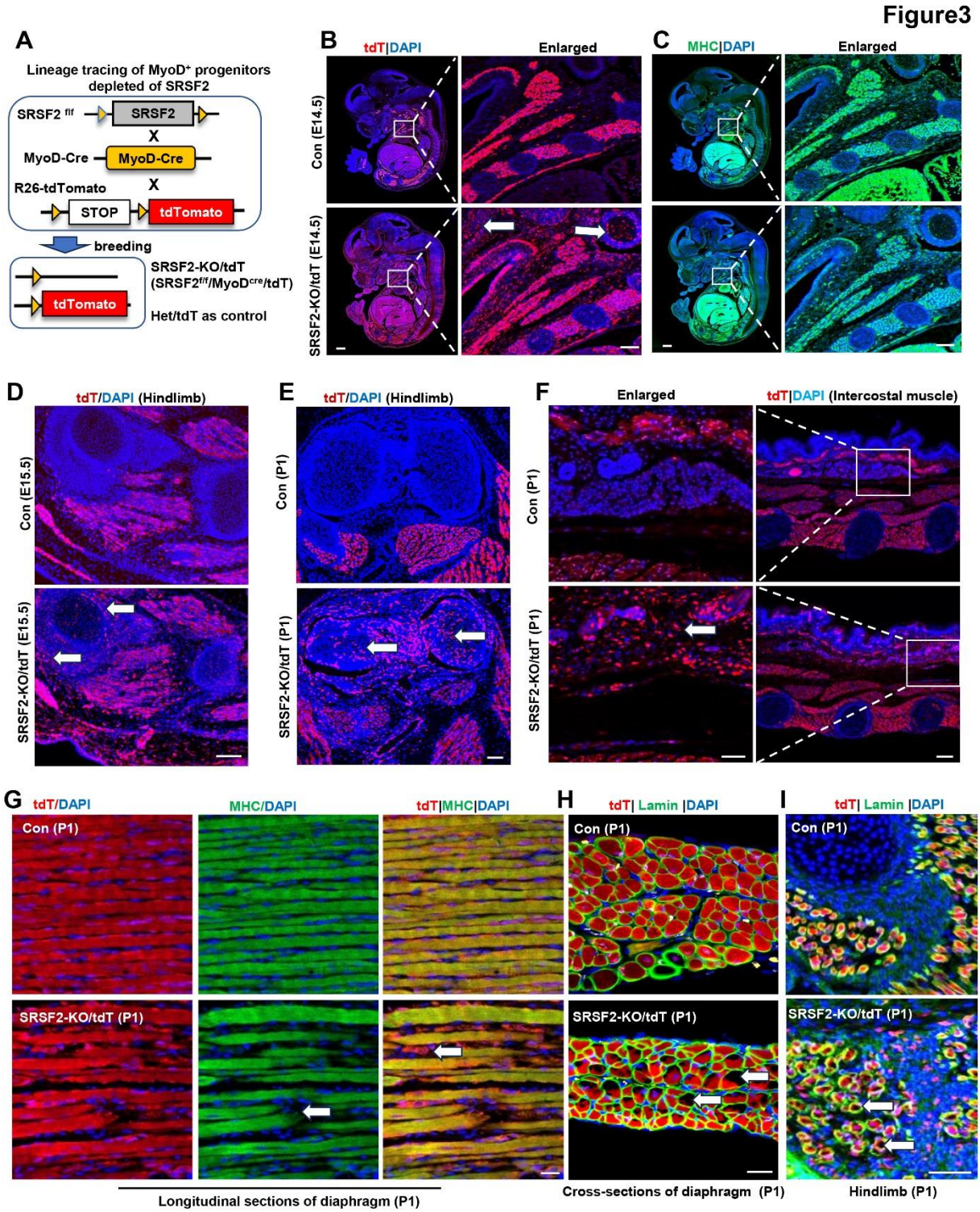

Figure 3. SRSF2-deficinent MyoD-derived cells migrated into non-skeletal muscle regions and displayed significant differentiation defects. (A) A schematic diagram of SRSF2-KO/tdT mice (SRSF2$^{f/f}$;MyoD^{Cre};tdT) was generated through the breeding SRSF2$^{f/f}$ mice with MyoD^{Cre} mice and Rosa26-tdTomato mice. SRSF2$^{f/w}$;MyoD^{cre};tdT mice served as the control group. (B) Representative confocal images of tdT (red)

staining on sagittal sections from E14.5 control and KO/tdT embryos. Scale bar is 500 μm. The red boxes indicated the enlarged images on the right, with a scale bar of 100 μm. (C) Representative confocal images of MHC (green) staining on sagittal sections from E14.5 control and KO/tdT embryos. Scale bars, 500 μm. White arrows indicated non-skeletal muscle regions. The enlarged images were shown on the right, with a scale bar of 100 μm. (D) Representative confocal images of tdT (red) staining in hindlimb sections from E15.5 mice. Scale bars, 100 μm. White arrows indicated non-skeletal muscle regions. (E) Representative confocal images of tdT (red) staining in hindlimb sections from P1 mice. Scale bars, 100 μm. White arrows indicated non-skeletal muscle regions. (F) Representative confocal images of tdT staining in transverse sections of intercostal muscle isolated from P1 mice. Scale bars, 200μm. Enlarged images were shown on the left with a scale bar of 50μm. (G) Representative confocal images of tdT (red) and MHC staining on longitudinal diaphragm sections from P1 mice. Scale bars, 20μm. White arrows indicate undifferentiated cells or tdT-labeled cells without MHC staining. (H) Representative confocal images of tdT (red) and Laminin (green) immunostaining in transverse diaphragm sections from P1 mice. Scale bars, 20μm. (I) Representative confocal images of tdT (red) and Laminin (green) immunostaining in hindlimb sections from P1 mice. Scale bars, 50μm. White arrows highlight cavities within tdT/Lamin labeled cells.

scRNA-seq analysis reveals distinct cell populations within the diaphragm

To further investigate the molecular mechanisms underlying effect of SRSF2 in myogenesis, we extracted diaphragms from newborn WT and SRSF2-KO mice, prepared single-cell suspensions, and conducted scRNA-seq using the 10X Genomics Chromium system (Fig. 4A). After rigorous quality control (Fig. S3), we obtained a final dataset consisting of 9506 WT cells and 11384 SRSF2-KO cells for downstream analysis. The resulting t-distributed stochastic neighbor embedding (t-SNE) analysis revealed 23 distinct cell clusters (Fig. S4). Utilizing the top 10 marker genes in each cell cluster, correlation analysis between different cell clusters (Fig. S5), and previously reported marker gene analysis, we successfully categorized the various cell types present in the diaphragm. These included fibroblasts, endothelial cells, skeletal muscle cells (SKM), mesothelial cells, immune cells, smooth muscle cells, tendon tenocytes, and glial cells (Fig. 4B-4D).

Evaluation of the cell composition proportions revealed no significant differences between WT and KO groups (Fig. 4E). Individual t-SNE plots demonstrated a notable reduction in SRSF2 expression specifically in SKM cells, while other cell types within

the diaphragm of SRSF2-KO group maintained similar levels of SRSF2 compared to the control (Fig. 4F).

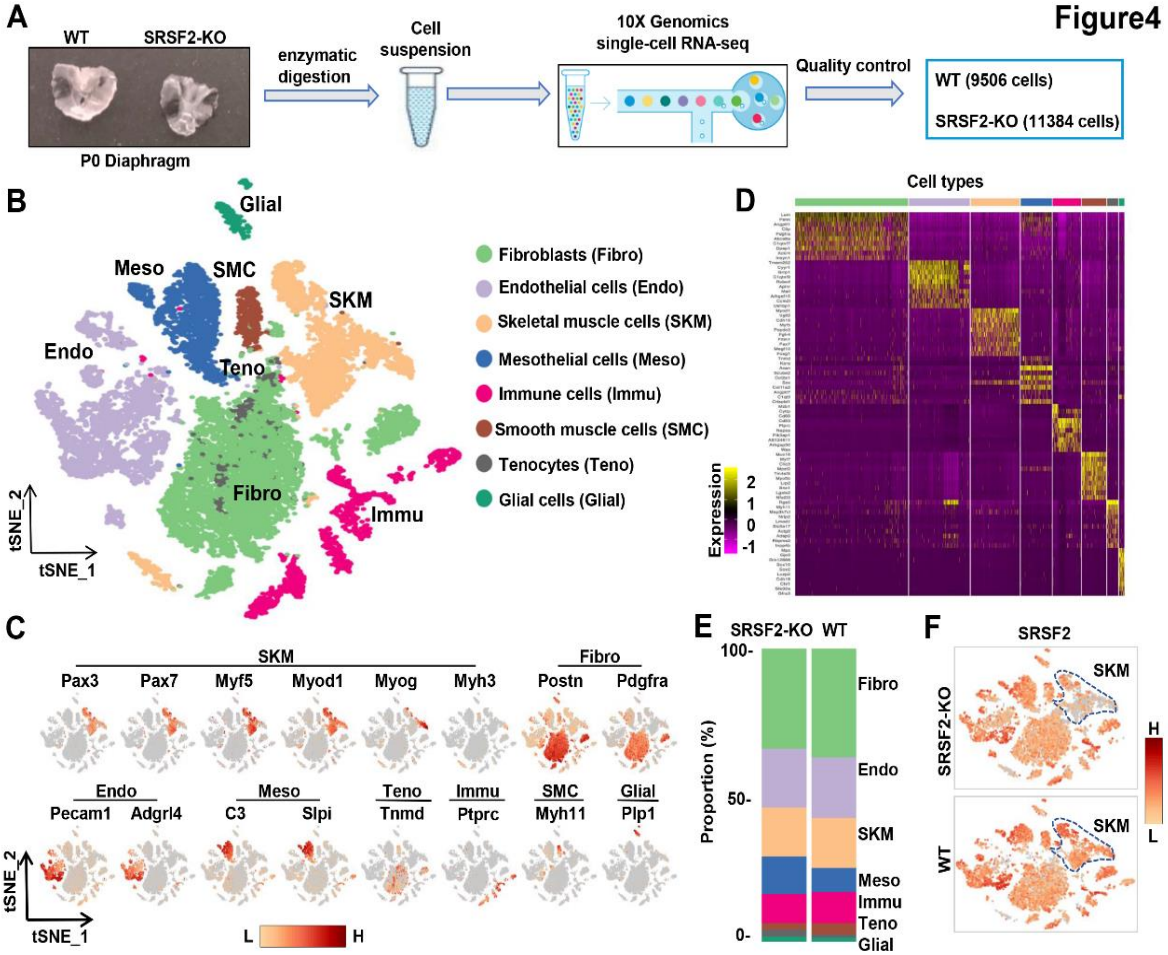

Figure 4. snRNA-seq analysis identifies distinct cell populations within P1 diaphragms. (A) Diagram of single-cell preparation from P1 diaphragms and processing using the 10X Genomics platform for single-cell RNA-sequencing analysis. (B) t-SNE plot showing 8 distinct cell populations identified in P1 WT and SRSF2-KO groups. Note that clusters expressing same marker genes were grouped into the same population. (C) t-SNE plot showing the expression of representative marker genes within distinct cell populations. (D)Heatmap showing the top 10 most differently expressed genes among 8 distinct cell populations. (E) Proportion comparison of cell populations between WT and SRSF2-KO groups. (F) The levels of SRSF2 are reduced in the SRSF2-KO skeletal muscle (SKM) cells compared to WT cells

Precocious differentiation was observed in SRSF2-deficient SKM population

We then conducted unsupervised cluster analysis specifically on the SKM population,

which led us to identify six subclusters (sC1 to sC6) with distinct transcriptomes (Fig. 5A and Fig. S6). As depicted in Fig. 5B, sC1 and sC2 exhibited similar levels of expression for the SC markers *Pax7* and *Myf5*. Notably, sC2 cells displayed elevated expression of *Myod1* and the proliferation marker *Mki67*, indicating their identity as cycling myoblasts (Cycling MB). In contrast, sC1 cells displayed low levels of *Myod1* expression and lacked *Mki67,* classifying them as non-cycling satellite cells (SCs). sC3 and sC4 cells were identified as committed MB and myocytes, respectively, based on their expression of differentiation markers such as *Myog* and *Ckm*. For subsequent analysis, sC5 and sC6 cells were excluded due to their lack of distinct identity.

Subsequently, we employed Monocle2 (Trapnell et al., 2014) to investigate the dynamic cell transitions during myogenesis. Our analysis revealed that it organized the four subclusters into two major trajectories (Fig. 5C). Cycling MBs (sC2) were positioned at the initiation of pseudotime trajectory, committed MB (sC3) and myocytes (sC4) were situated at the terminal phase of the differentiation branch, while non-cycling SCs (sC1) were positioned on the branch associated with quiescence. Our examination of dynamic gene expression profiles along the cycling to differentiation branch or the quiescence branch revealed distinct patterns (Fig. 5D). Differentiation-related genes such as *Acta1 Ckm, Myh8, Tnnt1,* and *Tnnt3,* were highly expressed at the end of the differentiation branch (Module1). Proliferation marker*s* including *Cdc20, Cdk1, Fbxo5, Mki67,* and *Prc1* were predominantly observed at the starting point of cycling (Module 2). QSC markers like *Gpx3*, *Myf5*, *Notch3, Hes1* and *Pax7* were enriched at the end of the quiescence branch (Module 3). Genes such as *Cdkn1a, Myog, Mymx, Mymk* and *Rb1* were highly expressed during the middle stage transitioning from cycling to the differentiation branch (Module 4). Thus, cycling MBs during perinatal myogenesis have two potential pathways: differentiation or quiescence.

Through the examination of separate t-SNE plots of SKM subclusters (Fig. 5E) and the analysis of proportions (Fig. 5F), several significant observations emerged. Firstly, the proportion of non-cycling SCs (sC1) was reduced in the SRSF2-KO group, and their distribution notably deviated from that of sC1 in the WT group. Furthermore, the proportion of committed MB (sC3) decreased, while the proportion of myocytes (sC4) increased in the KO group when compared to the control. Consistently, the expression of differentiation-related genes such as *Acta1*, *Myh8* and *Ckm* occurred earlier expression along the differentiation branch in the KO group as apposed to the WT group (Fig. 5G, left panel). In contrast, proliferation-related genes like *Mki67*, *Cdk1* and *Clspn* showed no expression at the end of the quiescence branch in the WT group, whereas their expression remained relatively high in the KO group (Fig. 5G, right panel). These findings collectively indicate a precocious differentiation process in the absence of SRSF2.

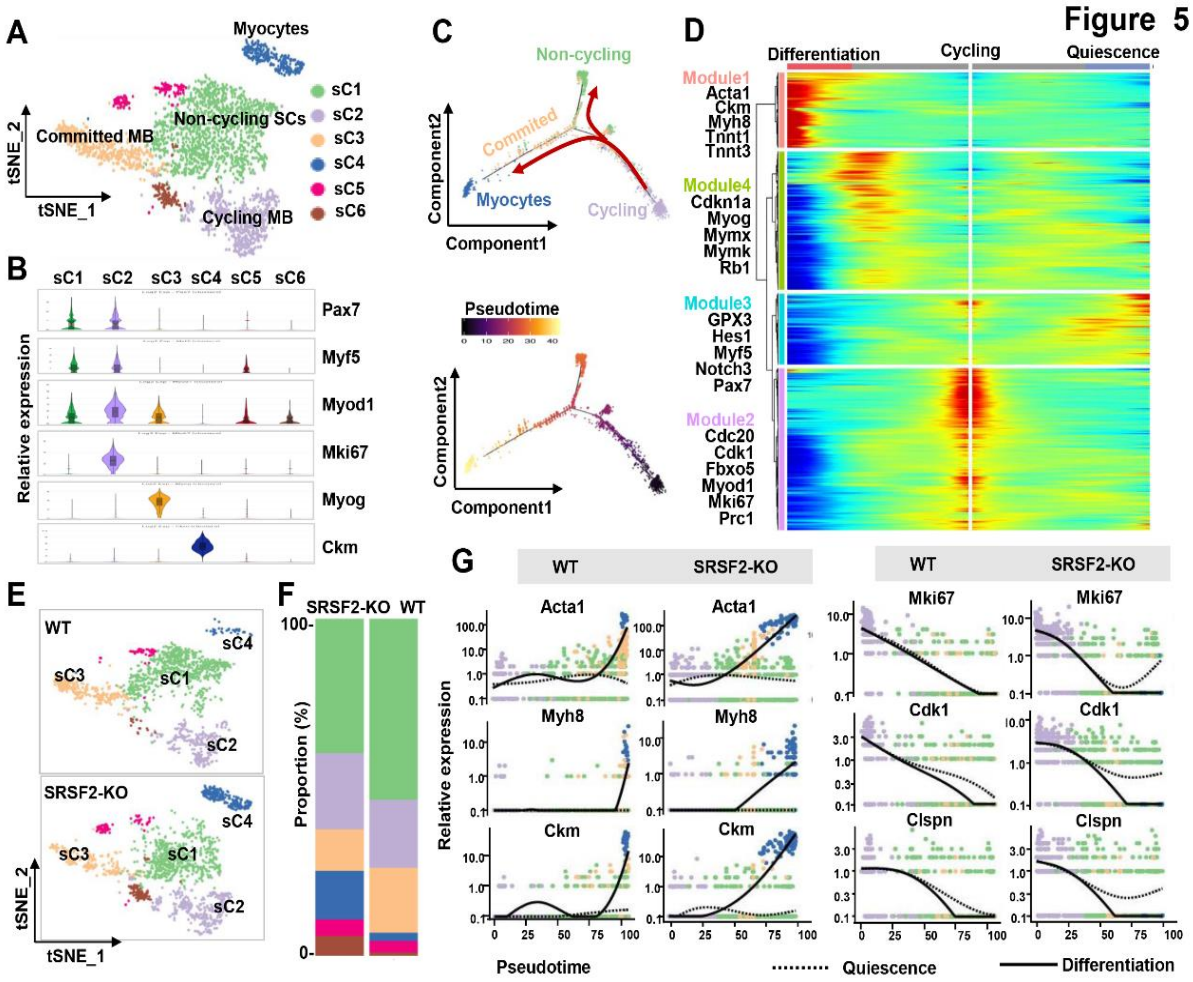

Figure 5. Loss of SRSF2 results in precocious differentiation of myoblasts. (A) The t-SNE plot reveals six distinct subclusters from WT and SRSF2-KO SKM cells. (B) Violin plot showing expression levels of the marker genes in the subclusters. (C) Pseudotime-ordered analysis of SKM subclusters, shown as arrangement of subclusters along the two branches of the pseudotime (top), and their pseudotime order (bottom). (D) Heatmap showing expression dynamics of marker genes along the pseudotime branches. Representative marker genes in the four expression modules along the pseudotime shown on the left to the heatmap. (E) Separate t-SNE subcluster projections of WT (top) and SRSF2-KO (bottom) SKM cells. (F) Proportion comparison of WT and SRSF2-KO SKM subclusters. (G) Plots showing the relative levels of marker genes of WT (left) and SRSF2-KO (right) along the differentiation and quiescence branches of the pseudotime, respectively.

Decreased ECM/cytoskeleton-related components, mitotic abnormalities, and defective differentiation were observed in the KO group

To further investigate the mechanisms underlying the observed precocious differentiation in KO myoblasts, we conducted an analysis of DEGs within subclusters, followed by a GO enrichment analysis. This analysis unveiled a substantial reduction in components associated with both the ECM and the cytoskeleton in the sC1, sC2 and sC3 cells of the KO group, as shown in Fig. 6A. Notably, significant alterations were also observed in terms related to “ameboidal-type cell migration” and “negative regulation of cell cycle” within in the sC2 cells of the KO group. Additionally, there was a noteworthy reduction in genes involved in Z-disc formation within the sC4 cells of the KO group.

The ECM architecture is composed of complex supramolecular fibrillar networks that define tissue specific cellular microenvironments. Genes encoding crucial collagen proteins for ECM structural integrity, such as Col1a2, Col6a2, and Col18a1, exhibited significant downregulation in sC1, sC2 and sC3 cells within the KO group (Fig. 6B). Moreover, other ECM-related genes, including Dpt (dermatopontin), Hmcn2 (hemicentin-2), Loxl1 and Loxl2 (lysyl oxidase-like 1 and 2), and Tnc (tenascin-C), all contributing to ECM composition and function, displayed significant downregulation in sC1, sC2 and sC3 of the KO group (Fig. 6B).

In addition, genes associated with “ameboidal-type cell migration” such as Acta2 (actin alpha 2), Pfn1 (profilin-1), Ran (Ras-related nuclear protein), and Thbs1

(Thrombospondin-1) showed notable decreases in expression levels in sC1, sC2, and sC3 cells of the KO group. Genes related to cytoskeleton organization, such as Tmsb4x (thymosin beta-4) and Tmsb10 (thymosin beta-10), were significantly downregulated in the KO group as well. Moreover, integrins, a family of cell adhesion receptors, mediating interactions between cells and the ECM, experienced significant downregulation in the KO group, particularly the expression of Itga7 and Itgb1, integrin subunits (Fig. 6C). This collective downregulation of ECM and cytoskeleton-related genes underscores the disruption in the molecular and structural interactions between myoblasts and their microenvironment in the KO group, potentially affecting cell migration, cell proliferation and differentiation.

Indeed, as illustrated in Fig. 6D, individual genes such as Aurka (Aurora kinase A), Birc5 (Survivin), Cetn3 (Centrin-3), Poc1a (POC1 centriolar protein A), Fbxo5 (F-box only protein 5), Nuf2 (NDC80 kinetochore complex component Nuf2), Mapre1 (Microtubule-associated protein RP/EB family member1), and Ttc28 (Tetratricopeptide repeat domain 28), play vital roles in regulating microtubule dynamics, spindle assembly, centriole and spindle pole formation, and mitotic progression control. These genes displayed decreased expression in proliferating myoblasts (sC2) of the KO group, indicating a disruption in normal cell division and spindle assembly processes. Mymk (myomaker) and Mymx (myomerge) are essential for myoblast fusion, resulting in multinucleated myotube formation. Interestingly, their expression, along with Myog, was significantly downregulated in committed myoblasts (sC3) of the KO group (Fig. 6E). On the other hand, Tcap (telethonin), involved in the assembly and maintenance of the Z-disc in skeletal muscle, showed increased expression in myocytes (sC4) of the KO group. This suggests the defective differentiation in the absence of SRSF1.

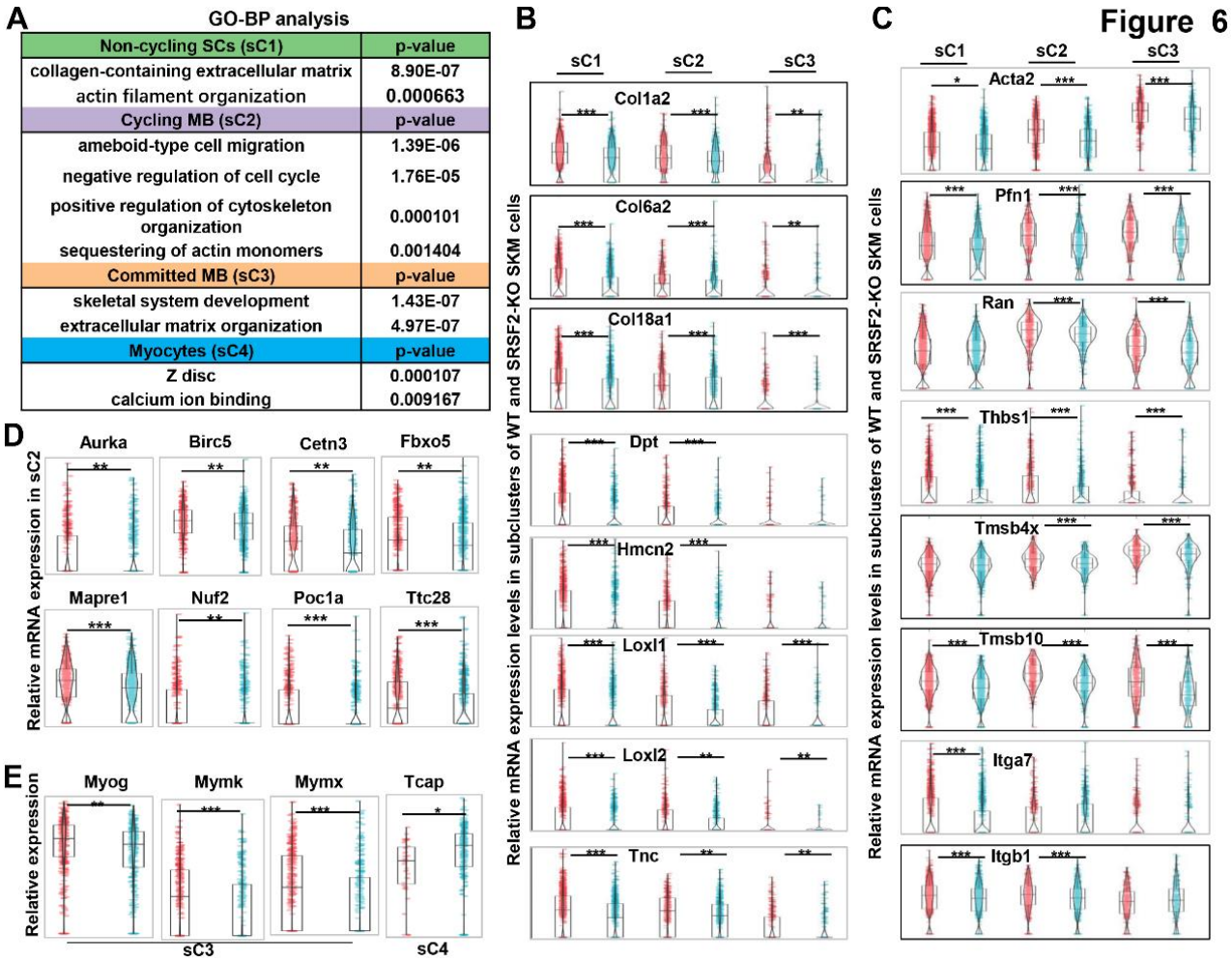

Figure 6. Decreased levels of ECM and cytoskeleton, along with mitosis abnormalities and differentiation defects, were observed in the KO group. (A) GO analysis of DEGs within four subclusters of SKM cells. (B) Violin plots showing relative expression levels of ECM components between WT and KO subclusters. (C) Violin plots showing relative expression levels of cytoskeleton-related genes between WT and KO subclusters. (D) Violin plots showing relative expression levels of mitosis-related genes between WT and KO sC2 cells. (E) Violin plots showing relative expression levels of differentiation-related genes between WT and KO subclusters.

SRSF2 regulates Aurka expression to control differentiation of C2C12 myoblasts

Previous reports have demonstrated that SRSF2 functions as a potent transcription activator (Cheng et al., 2016; Ji et al., 2013). To investigate this further, we utilized a public database to search for SRSF2 ChIP-seq signals on genes that were downregulated in the SRSF2-deficient myoblasts, as revealed by scRNA-seq analysis.

Among these genes, Aurka, pivotal in regulating cell cycle progression and microtubule dynamics, exhibited strong SRSF2 binding signals in its promoter regions (Fig. 7A). ChIP-qPCR analysis provided additional evidence that SRSF2 directly bind to its promoter regions (Fig. 7B). Moreover, knockdown of SRSF2 had a significant impact on the reduction of Aurka protein levels in C2C12 myoblasts (Fig. 7C, left panel). In contrast, when Aurka was knocked down, it did not affect the protein levels of SRSF2 (Fig. 7C, right panel), confirming that SRSF2 acts upstream of Aurka.

Intriguingly, both SRSF2 and Aurka knockdowns resulted in decreased protein levels of cell-cycle- and proliferation-related genes such as Cdk1, pRb, p-pRb, p-Akt, while simultaneously increasing the expression of the cell-cycle inhibitor p27 and autophagy p62 (Fig. 7C). Further analysis using RT-qPCR revealed that both knockdowns led to reduced levels of mitosis-related genes like Fbxo5, Nuf2, Poc1a, Ranbp1 and Spdl1 (Fig. 7D and 7E). Immunostaining analysis with phalloidin staining revealed both knockdowns induced significant alterations in the cytoskeleton and resulted in the formation of elongated pseudopods in the cells (Fig. 7F).

Next, we aimed to investigate whether knockdown of SRSF2 and Aurka affect C2C12 cell differentiation. Following transfection of C2C12 cells with indicated siRNAs for 48 hours, cells were switched from growth medium to differentiation medium. Immunostaining with differentiation markers Myog and MHC revealed that both SRSF2 and Aurka knockdowns significantly impeded myogenic differentiation of C2C12 cells. While long multinucleated myotubes were observed in control cells, only short and unaligned myotubes were present following SRSF2 or Aurka knockdowns (Fig. 7G and 7H, lanes 1-6). Given that Aurka was an important target of SRSF2, we decided to test if Aurka overexpression could rescue differentiation defects seen in SRSF2 depletion. To this end, we co-transfected C2C12 cells with siSRSF2 and an Aurka-overexpressing plasmid for 48 hours and then differentiated the cells for 3 days (Fig. 7H, lanes 7-10). Overexpression of HA-tagged Aurka significantly rescued differentiation defects induced by downregulation of SRSF2, as evidenced by increased staining for Myog and MHC observed in Aurka-overexpressing cells (Fig. 7I).

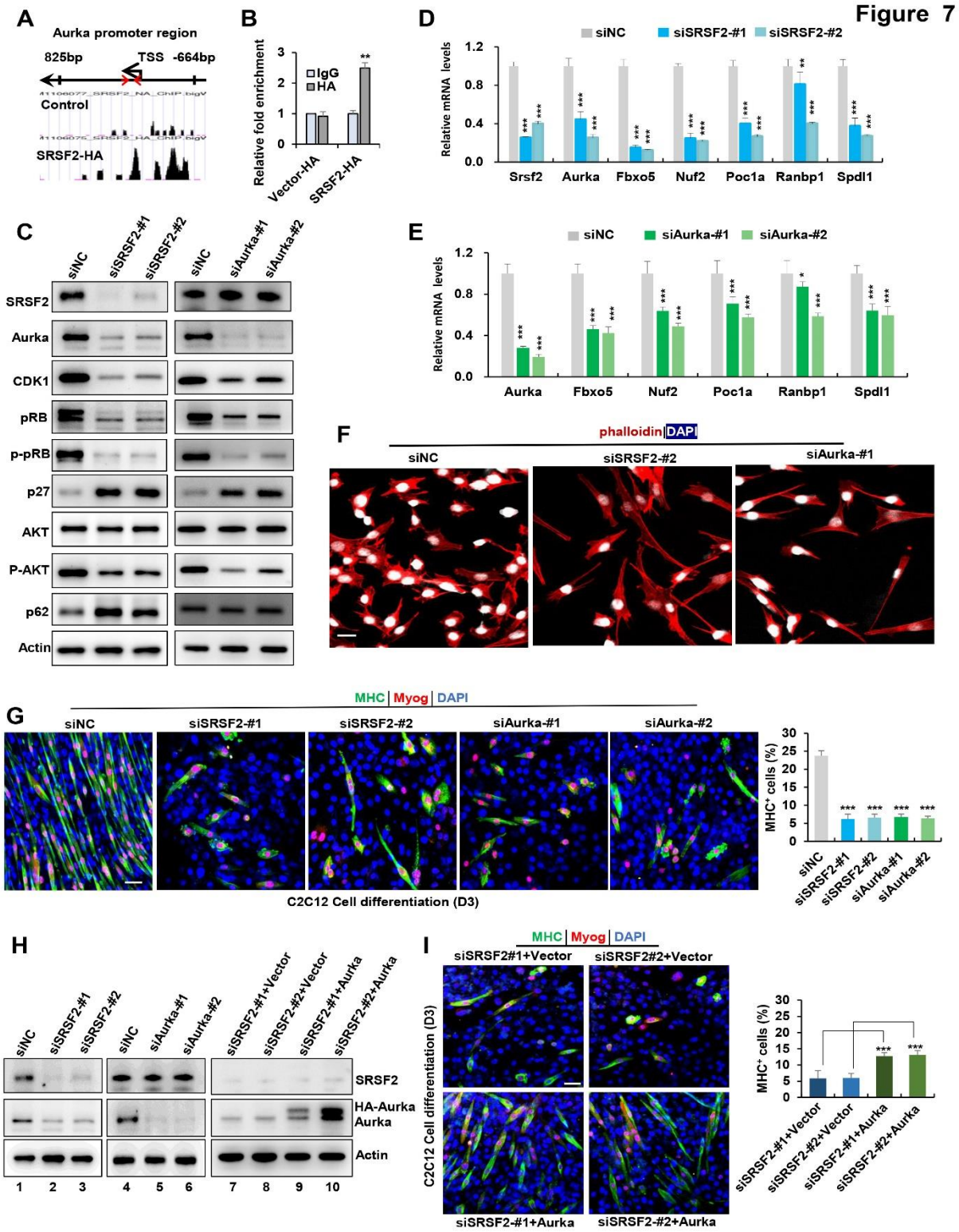

Figure 7. SRSF2 regulates Aurka expression to control mitotic processes and differentiation of C2C12 myoblasts. (A) UCSC genome browser screenshots illustrate SRSF2 ChIP-seq signals on the Aurka gene. A pair of primers is highlighted by red arrows, indicating their relative positions from the transcription start sites (TSS) within the Aurka promoter region on the top. (B) ChIP-qPCR analysis quantifies SRSF2-bound Aurka promoter regions in C2C12 myoblasts, with relative enrichment

folds normalized to the IgG group. (C) Western blot analysis for indicated proteins in C2C12 cells transiently transfected with siRNAs against SRSF2 (siSRSF2-#1, siSRSF2-#2) for 48 hours (left) or against Aurka (siAurka-#1, siAurka-#2) for 48 hours (right). (D) qPCR analysis of spindle formation-related genes in C2C12 cells following SRSF2 knockdown for 48 hours. (E) qPCR analysis of spindle formation-related genes in C2C12 cells with Aurka knockdown for 48 hours. (F) Immunostaining of phalloidin(red) and DAPI (blue) after SRSF2 or Aurka knockdown. Scale bars, 20μm. (G) Representative confocal images of MHC (green), Myog (red), and DAPI (blue) immunostaining in C2C12 cells. Scale bars, 50 μm. C2C12 cells were transfected with indicated siRNAs, then induced into differentiation for 3 days. Qualification of MHC+ cells were shown on the right graphs. (H) Western blot analysis was performed using whole cell extracts isolated from C2C12 cells transfected with indicated siRNAs (lanes 1-6), or with the indicated siRNAs along with either vector plasmid or Aurka plasmid, respectively (lanes 7-10). (I) Representative confocal images of MHC (green), Myog (red), and DAPI (blue) immunostaining in C2C12 cells. Scale bars, 50 μm. C2C12 cells were co-transfected with the indicated siRNAs along with either vector plasmid or Aurka plasmid, respectively, then induced into differentiation for 3 days. Qualification of MHC+ cells were shown on the right graphs.

SRSF1 plays a crucial role in the regulation of alternative splicing in genes associated with human skeletal muscle diseases

SRSF2 serves a dual role, not only as a transcriptional regulator but also as a key player in alternative splicing. To explore its involvement in skeletal muscle development, we utilized the RNA-seq platform to investigate its role in the regulation of AS events. Our extensive analysis revealed a total of 23 AS events with significant changes in the KO muscle samples. Interestingly, several targets affected by SRSF2, such as BIN1 (bridging interactor 1), DMPK(Dystrophin myotonica-protein kinase), FHL1(Four-and-a-half Lim domains protein 1), and LDB3(Lim domain binding 3), have been linked to conditions such as centronuclear myopathy, myotonic dystrophy, various X-linked muscle diseases, and myofibrillar myopathy (Nicot et al., 2007; Pathak et al., 2021; Prokic et al., 2014; Thomas et al., 2018) (Fig. 8A). Notably, the deficiency of SRSF2 in the KO muscle samples led to exon 17 skipping in Bin1, exon5 skipping in Fhl1, exon 9 skipping in Ldb3, and the inclusion of the proximal 3'-alternative exon 14 in DMPK (Fig. 8B). These findings proved valuable insights into the potential role of SRSF2 in AS regulation and its connection to the development of human skeletal

muscle diseases.

Nrap, Pdlim3, Pdlim7 and Trim54 are well-known for their contributions to muscle development and cytoskeletal structural integration (D'Cruz et al., 2016; Jirka et al., 2019; Lodka et al., 2016; Yin et al., 2020) (Fig. 8A). Notably, SRSF2 deficiency resulted in specific alterations in their splicing patterns, including exon 12 skipping in Nrap, exon 5 skipping in Pdlim3, exon4 skipping of Trim54, and inclusion of exon 5 in Pdlim7(Fig. 8C). Genes associated with apoptosis and mitochondria, such as Aamdc, Dap3 and Dnm1l(Golden et al., 2021; Tong et al., 2023; Xiao et al., 2015) were found to be under the splicing regulation of SRSF2. This led to exon4 skipping in Aamdc and exon 11 skipping in Dap3, while exon 17 was include in Dnm1l in the KO group (Fig. 8A and 8D). Furthermore, Ppp3ca and Ppp3cb play vital roles in calcium handling in skeletal muscle cells(Brinegar et al., 2017). In the absence of SRSF2, exon 13 of Ppp3ca and both exon 10a and exon13 of Ppp3cb were skipped (Fig. 8A and 8D). These findings strongly indicated that these dysregulate AS events play a contributing role in the effects of SRSF2 during skeletal muscle development.

Next, we aimed to analyze whether knockdown of SRSF2 affect these AS events in C2C12 cells. As illustrated in Fig. 8E, SRSF2 knockdown resulted in similar exon changes in genes such as Bin1, Ldb3, Trim54, Dap3, Dnm1l in C2C12 cells as observed in KO skeletal muscles. Given that dysregulated splicing of BIN1 is associated with muscle weakness in myotonic dystrophy (DM)(Fugier et al., 2011), we directed our focus towards Bin1 variants for further analysis. As shown, BIN1 contains 20 exons, with alternative exons regulated in different tissues (Fig. 8F). Notably, exon7 and exons12-16 are excluded from human skeletal muscles, while exon 11 is excluded from normal brain tissues and DM skeletal muscles. However, we did not detect any alteration in exon 11 skipping in both SRSF2-knockdown cells and SRSF2-KO skeletal muscles (Fig. 8E and 8G). Instead, our data demonstrated that SRSF2 is responsible for exon 17 inclusion in both skeletal muscles and C2C12 cells (Fig. 8B and 8E). To investigate whether exon17 skipping of Bin1 is involved in C2C12 differentiation, we designed siRNAs specifically targeting against Bin1 exon17. Both siBin1-#1 and

siBin1-#2 significantly decreased the levels of exon17-containing variants in C2C12 cells (Fig. 8H). The decreased staining for Myog and MHC strongly suggested impaired C2C12 differentiation following the specific knockdown of the Bin1-exon17 variant (Fig. 8I). These findings highlighted the critical role of SRSF2-regulated exon17 inclusion of Bin1 in C2C12 cell differentiation.

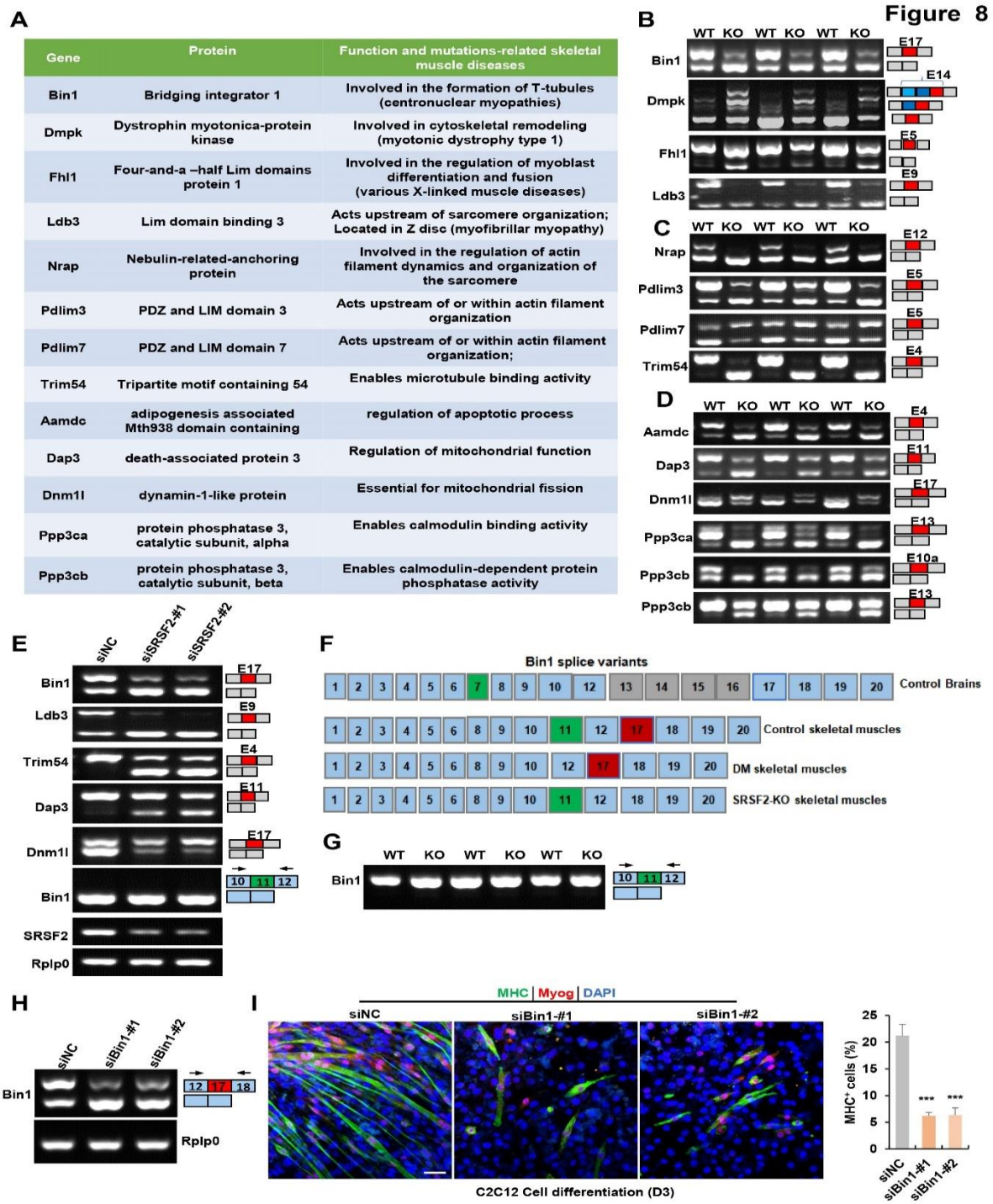

Gene	Protein	Function and mutations-related skeletal muscle diseases
Bin1	Bridging integrator 1	Involved in the formation of T-tubules (centronuclear myopathies)
Dmpk	Dystrophin myotonica-protein kinase	Involved in cytoskeletal remodeling (myotonic dystrophy type 1)
Fhl1	Four-and-a –half Lim domains protein 1	Involved in the regulation of myoblast differentiation and fusion (various X-linked muscle diseases)
Ldb3	Lim domain binding 3	Acts upstream of sarcomere organization; Located in Z disc (myofibrillar myopathy)
Nrap	Nebulin-related-anchoring protein	Involved in the regulation of actin filament dynamics and organization of the sarcomere
Pdlim3	PDZ and LIM domain 3	Acts upstream of or within actin filament organization
Pdlim7	PDZ and LIM domain 7	Acts upstream of or within actin filament organization;
Trim54	Tripartite motif containing 54	Enables microtubule binding activity
Aamdc	adipogenesis associated Mth938 domain containing	regulation of apoptotic process
Dap3	death-associated protein 3	Regulation of mitochondrial function
Dnm1l	dynamin-1-like protein	Essential for mitochondrial fission
Ppp3ca	protein phosphatase 3, catalytic subunit, alpha	Enables calmodulin binding activity
Ppp3cb	protein phosphatase 3, catalytic subunit, beta	Enables calmodulin-dependent protein phosphatase activity

Figure 8. Alternative splicing events affected by SRSF2 during skeletal muscle development. (A) A table displaying genes alternatively spliced by SRSF2 during skeletal muscle development. (B) RT-PCR analysis of AS events observed in Bin1, Dmpk, Fhl1 and Ldb3 genes due to the absence of SRSF2, using total RNA isolated from three independent WT and KO samples. Alternative exons are highlighted in red with their respective exon number. Note that there were three 3' alternative sites within exon14 of Dmpk. SRSF2 deficiency resulted in selection of the proximal 3' site, while the presence of SRSF1 leads to the inclusion of the distal 3' site. (C) RT-PCR analysis of AS events observed in Nrap, Pdlim3, Pdlim7 and Trim54 genes in three independent WT and KO skeletal muscle samples. (D) RT-PCR analysis of AS events observed in Aamdc, Dap3, Dnm1l, Ppp3ca and Ppp3cb genes in three independent WT and KO skeletal muscle samples. (E) RT-PCR analysis of AS events observed in indicated targets following knockdown of SRSF2 in C2C12 cells for 48 hours. (F) Diagram of Bin1 splice variants present in both normal and diseased tissues. Note that green, red or gray exons represent alternative exons, while slight blue exons are constitutive. (G) RT-PCR analysis of Bin1 exon 11 inclusion in three independent WT and KO skeletal muscle samples. (H) RT-PCR analysis was conducted to assess the levels of Bin1 exon 17-containing and exon 17-lacking variants after transfection with siBin1-#1 or siBin1-#2 in C2C12 cells for 48 hours. The black arrows indicate primer positions. (I) Representative confocal images of MHC (green), Myog (red), and DAPI (blue) immunostaining in C2C12 cells. Scale bars, 50 μm. C2C12 cells were transfected with siBin1 for 48 hours, then induced into differentiation for 3 days. Quantification of MHC+ cells were shown on the right graphs.

Discussion

During embryonic skeletal muscle development, Myf5+ progenitors play a pivotal role in expanding the myogenic progenitor pool and migrating from somites to muscle-forming regions, establishing early muscle primordia [5b]. Notably, SRSF2 emerges as a critical regulator that inhibits apoptosis in My5+progenitors and maintain their migratory capability during embryonic skeletal muscle development. The absence of SRSF2 in Myf5+ progenitors leads to a high rate of myoblasts apoptosis at embryonic day E12.5, as well as aberrant migration, ultimately resulting in the complete loss of mature myofibers.

MyoD+ progenitors contribute to additional migration within muscle primordia, as they move to their final destinations within developing muscle tissues. They exhibit

high efficiency in differentiation into myotubes and muscle fibers. Deletion of SRSF2 in MyoD+ progenitors markedly disrupts their ability to migrate in a specific direction and subsequently impairs their differentiation process.

scRNA-seq analysis revealed substantial diversity within the fetal skeletal muscle cell population in the diaphragm. This diversity included non-cycling SCs, activated myoblasts, cycling myoblasts, committed myoblasts and myocytes. Our findings aligned with the observed diversity in muscle progenitors derived from human-induced pluripotent stem cells (Nalbandian et al., 2022). Notably, the deficiency of SRSF2 resulted in an increased number of myocytes while simultaneously reducing the population of committed myoblasts. In the context of skeletal muscle differentiation, Myh8, Ckm and Acta1 are critical for the formation of muscle fibers(Nowak et al., 2013; Schiaffino et al., 2015). Both Myomaker and Myomerger proteins directly control the myogenic fusion process(Chen et al., 2020). However, the expression of Myh8, Ckm and Acta1 was significantly advanced at earlier stage in the differentiation process, while there was a concurrent downregulation of MyoK and Myox in the absence of SRSF2. This suggests that enhanced differentiation was defective in the KO group.

scRNA-seq analysis further revealed significant effects of SRSF2 on the downregulation of ECM components, genes associated with ameboid-type cell migration, and cytoskeleton organization. The reduction of both ECM and cytoskeleton components has a significant impact on myoblast migration, cell division and differentiation(Osses *et al.*, 2009; Zhang *et al.*, 2021). Notably, one of the targets regulated by SRSF2 is Aurka, a serine/threonine kinase that plays a crucial role in regulating cell division processes via regulation of mitosis(Du et al., 2021). The chromosome passenger complex, which includes Aurka, inhibits the shrinkage of microtubules, thereby promoting cell growth(Namgoong and Kim, 2018). Our data revealed that knockdown of Aurka led to reduced cell proliferation, disrupted cytoskeleton, and impaired differentiation, which mirrored the effects observed with SRSF2 knockdown. Importantly, overexpression of HA-Aurka in SRSF2-knockdown cells substantially rescued the differentiation defects observed following SRSF2

knockdown. These findings provided evidence that SRSF2- regulated Aurka expression is critical for differentiation of C2C12 cells.

In addition to its role in transcription regulation, SRSF2 also has a significant impact on the alternative splicing regulation of genes related to human skeletal muscle diseases. Dysregulated alternative splicing of BIN1 has been linked to T-tubule alterations and muscle weakness in myotonic dystrophy(Fugier *et al.*, 2011). BIN1 is involved in forming tubular of membrane invaginations and is critical for the development of muscle T-tubules, specialized membrane structures essential for excitation-contraction coupling. Mutations in the BIN1 gene can lead to centronuclear myopathy, a condition that shares some histopathological features with myotonic dystrophy. MBNL1 binds the BIN1 pre-mRNA and regulates its alternative splicing. Skipping of exon11 in BIN1 results in the expression of an inactive form of BIN1 lacking phosphatidylinositol 5-phosphate-binding and membrane-tubulating activities. Notably, the deletion of SRSF2 resulted in centronuclear features in skeletal muscle, and induced exon17 skipping in Bin1, which resides within the Myc-binding domain of Bin1 protein. Targeted knockdown of the Bin1 exon17-containing variant significantly disrupted C2C12 cell differentiation. Further investigation is imperative to comprehend the involvement of SRSF2 and its regulation of exon17 inclusion in BIN1 in human skeletal muscle diseases.

In summary, our research provides valuable insights into the role of SRSF2 in governing MyoD progenitors to specific muscle regions, thereby controlling myogenic differentiation through the regulation of targeted gens and alternative splicing during skeletal muscle development.

Materials and Methods

Generation of conditional knockout mice

SRSF2$^{f/f}$ mice were obtained from Dr. Fu at Westlake University. The SRSF2$^{f/f}$ mice were bred with transgenic C57BL/6J mice that express Cre recombinase under the control of the Myod1 promoter. The resulting offspring (SRSF2$^{f/w}$;MyoD^{Cre}) were then

bred with SRSF2$^{f/f}$ mice to generate SRSF2 knockout mice SRSF2$^{f/f}$;MyoD^{Cre} (SRSF2-KO) The SRSF2$^{f/f}$/tdT mice used in this study were previously described(Guo *et al.*, 2022). These mice were crossed with SRSF2$^{f/w}$/MyoD^{Cre} mice to generate control mice (SRSF2$^{f/w}$;MyoD^{Cre};tdT) and SRSF2-KO/tdT mice (SRSF2$^{f/f}$;MyoD^{Cre};tdT mice). All animal experiments were conducted in accordance with the guidelines of the Institutional Animal Care and Use Committee of Shanghai Institute of Nutrition and Health, Chinese Academy of Sciences.

HE staining and Immunofluorescence staining

Mouse skeletal muscle tissues were fixed in 4% paraformaldehyde and embedded in paraffin or OCT. 7μm-thick sections were stained with hematoxylin and eosin following standard protocols. For immunofluorescence on the paraffin-embedded tissues, 7μm-thick sections were deparaffinized in xylol for 30 minutes and rehydrated in a gradient of ethanol (100%, 95%, 75%, 50%) for 15 minutes, followed by antigen retrieval. The sections were then blocked with 5% normal goat serum (Santa Cruz Biotechnology) for 1hour and incubated with primary antibodies overnight at 4°C. Subsequently, the secondary antibody was applied for 1 hour, and DAPI staining was performed for 10 minutes. For immunofluorescence on the OCT-embedded tissues, 5μm-thick sections were washed in PBS for 15 minutes to remove the OCT, and then the sections were blocked and stained similarly to the paraffin sections. Immunofluorescence images were acquired using a Zeiss LSM880NLO Confocal Microscope and the ZEN software. The detailed information of the antibodies used is listed in Table S1.

Transmission electron microscopy

Diaphragms from P1 WT and SRSF2-KO mice were fixed overnight at 4°C in a 2.5% glutaraldehyde solution, followed by four 15-minute PBS washes. Subsequently, they underwent dehydration in an ascending ethanol series (50%, 70%, 80%, and 90%) for 15 minutes each, with two rounds of 100% ethanol dehydration for 20 minutes each. The diaphragms were cleared twice with acetone for 15 minutes each and underwent a series of infiltrations. First, they were in an acetone:embedding medium (2:1 v/v) solution for 1 hour, followed by a solution of acetone:embedding medium (1:2 v/v) for

4 hours. Afterward, they were infiltrated twice with pure embedding medium for 20-24 hours each. After infiltration, the diaphragms were placed into a mold filled with pure embedding medium and polymerized at 65°C for over 48 hours. The embedded block was trimmed into a trapezoid shape to ensure a sample surface area less than 0.2mm x 0.2mm. Ultrathin sections with 70nm in thickness were cut and stained with uranyl acetate for 10 minutes, followed by lead citrate for another 10 minutes, with washing steps in between. Finally, the sections were examined under the transmission electron microscope.

RNA-seq analyses

The total RNAs were extracted from diaphragms of newborn mice and subjected to high-throughput transcriptome analysis using RNA sequencing (RNA-SEQ). Paired-end (PE) sequencing was performed using Next-Generation Sequencing (NGS) on the Illumina HiSeq sequencing platform. The raw data was processed using Cutadapt to trim 3' adapter sequences and reads with an average quality score below Q20 were removed, resulting in clean data. The clean data reads were then aligned to the mouse transcriptome (GRCm38/mm10) using HISAT2, an updated version of TopHat2. Gene expression levels were calculated based on the alignment results. Further analyses, including differential expression, enrichment, and alternative splicing analyses, were performed on the samples. DESeq was used for differential analysis of gene expression and GO enrichment analysis was performed using topGO. The alternative splicing analysis was performed with rMATs. The raw data sets have been submitted to the SRA database with the accession number PRJNA974218.

RNA extraction, RT-PCR and qPCR

Total RNA was extracted from diaphragm tissues or C2C12 cells using Trizol Reagent (Invitrogen). The RNA was then reverse-transcribed into cDNA using the High-Capacity cDNA Reverse Transcription kit (Applied Biosystems). For differential expression analysis, qPCR was performed with the SYBR Premix Ex Taq kit (TaKaRa) with Rplp0 serving as the internal control. For alternative splicing analysis, RT-PCR

was conducted following the previously described method(Cheng *et al.*, 2016; Zhou et al., 2014). The primer sequences used in this study are listed in Table S2 & Table S3.

Preparation of Single Cell Suspension and scRNA-seq

The diaphragms were isolated from P1 SRSF2$^{f/f}$ and SRSF2$^{f/f}$;MyoD^{Cre} mice. The diaphragms were cut to pieces, and then digested in a solution containing 0.2% (wt/vol) collagenase-type XI (Sigma-Aldrich) and 2.4 U mL^{-1} dispase Ⅱ (Invitrogen) in DMEM at 37°C for 45 minutes. The digested tissue was filtered through a 40-μm cell strainer and a 70-μm cell strainer. The cells were then centrifuged, resuspended in a 20% FBS/PBS buffer, and counted using an automated cell counter. The cells were loaded onto a droplet-based library prep platform Chromium (10X Genomics) with a Chromium Single Cell Reagent Kit following the instructions provided in the protocol. Sequencing was performed on an Illumina Nova 6000 using150-base pair paired-end reads. The sequencing and bioinformatics analysis were carried out by OE Biotech Co., Ltd. (Shanghai, China). All statistical analyses, unless otherwise specified, were performed using R. The resulting datasets have been submitted to the GEO database with the accession number GSE233227.

scRNA-seq Data Preprocessing

The Cell Ranger software pipeline (10X Genomics, version5.0.0) was utilized to assess data quality statistics on the raw data and map reads to the reference genome, resulting in a matrix of gene counts versus cells. Cells of low quality, such as double capture cells, multiple capture cells, or cells with more than 10% of counts from mitochondrial genes, were filtered out based on the nUMI, nGene, and percent.mito criteria using the R package Seurat (version 3.1.1). After applying these quality control measures, a total of 12,592 cells from the WT group and 14,875 cells from the SRSF2-KO group were available for further analysis. The library size was normalized using the NormalizeData function in Seurat, and dimensionality reduction was performed using the RunPCA function. Cell clusters were identified using the FindCluster in Seurat, and visualized using a 2-dimensional t-distributed stochastic neighbor embedding (t-SNE) algorithm with the RunSNE function. Marker genes for each cluster were identified using the

FindAllMarkers function, and cell types were manually determined based on cluster-specific marker genes and known marker genes. Differentially expressed genes (DEGs) were identified using the FindMarkers function (test.use = MAST) in Seurat (P value < 0.05 and | log2foldchange | > 0.58). Additionally, GO enrichment and KEGG pathway enrichment analyses of DEGs were conducted using R package based on the hypergeometric distribution.

Pseudotime Analysis

The developmental pseudotime was determined using the Monocle2 package (version 2.9.0)(Trapnell *et al.*, 2014). The raw count was first converted from a Seurat object into a CellDataSet object using the importCDS function in Monocle. The differentialGeneTest function of the Monocle2 package was then used to select ordering genes (qval < 0.01) that were likely to be informative in the ordering of cells along the pseudotime trajectory. Dimensional reduction clustering analysis was performed using the reduceDimension function, followed by trajectory inference with the orderCells function using default parameters. Gene expression was plotted using the plot_genes_in_pseudotime function to track changes over pseudo-time.

Cell culture, Differentiation, Transfection, and Immunostaining

C2C12 cells were cultured in DMEM supplemented with 10% fetal bovine serum. Transient transfection of C2C12 cells were performed using siRNA or plasmids. The Aurka overexpression plasmid was constructed using the longest NM isoform and inserted into the pCDNA3.0-HA plasmid vector. Myogenic differentiation of C2C12 cells was activated by replacing the growth medium with a differentiation medium (DMEM supplemented with 2% horse serum). The transfection was carried out using Lipofectamine RNAiMAX or Lipofectamine 200, both from Invitrogen, following the manufacturer's protocol. After 48 hours of transfection, or induction into differentiation for 3 days, the cells were fixed with 4% paraformaldehyde for 15 minutes. Then, permeabilization was done using 0.1% Triton X-100, and the cells were blocked with 5% normal goat serum for 1 hour. Subsequent staining was performed following the

same protocol as tissue immunofluorescence staining. The siRNA sequences used for RNA interference can be found in Table S4.

Western blot analysis

For western blot analysis, proteins were collected from C2C12 cells using RIPA lysis buffer (Thermo Scientific) supplemented with a complete protease inhibitor cocktail (Roche). After quantification, equal amounts of proteins were subjected to immunoblotting. The primary antibodies used in this study were listed in Table S1.

Chromatin Immunoprecipitation Assays (ChIP-qPCR)

ChIP-qPCR analysis was conducted to identify potential SRSF2 binding sites on the Aurka promoter regions. The biding site information was obtained from the Gene Expression Omnibus (GEO) database, specifically accession numbers GSM1106075 and GSM1106077. Two pairs of primers were designed based on this information for the ChIP-qPCR analysis. C2C12 cells were transiently transfected with SRSF2-HA and vector-HA plasmids for 48 hours. ChIP was performed using a Magna ChIP kit (Millipore; catalog no. MAGNA0017) following the manufacturer's instructions. Immunoprecipitation was carried out using anti-HA antibodies (Abcam), while normal mouse IgG served as a negative control. Quantification of the immunoprecipitated DNA and input DNA were done through qPCR analysis. Detailed information regarding the antibodies can be found in Table S1 of the Supporting Information, while the primer sequences used in this study are listed in Table S5.

Statistical Analysis

The data presented in the histograms were obtained from at least three independent experiments and are represented as the mean ± standard deviation (SD). Statistical difference between groups was determined for using a two-tailed unpaired Student's t-test. A p-value of $*p < 0.05$, $**p < 0.01$, and $***p < 0.001$ was considered statistically significant.

Acknowledgements

This work was supported by grants from the National Key R&D Program of China (No.

2021YFC2103001, for Y.F.), the Shandong Province Natural Science Foundation (ZR2021QH151 for X.Y.), the Research Fund for Lin He's Academician Workstation of New Medicine and Clinical Translation in Jining Medical University (JYHL2022MS26 for H.D.), the Shanghai Scientific Research Project (19JC1416000 for Y.F.), and the National Natural Science Foundation (31870819 and 31570818 for Y.F.). We thank Dr. Yongbing Ba and Lian Li (OE Biotech Co., Ltd, Shanghai, China) for assistance with bioinformatics analysis.

Author Contributions

R.S, R.G. and Y.F. designed research and analyzed data; R.S., R.G., H.D., Q.P., N.Y., Z.Z., Z.X., and X.Y. performed research. Z.L. helped with confocal images. R.S., R.G. and Y.F. wrote the paper. All authors reviewed and edited the manuscript.

Declaration of Interests

The authors declare no competing interests.

Reference:

Braun, T., and Gautel, M. (2011). Transcriptional mechanisms regulating skeletal muscle differentiation, growth and homeostasis. Nat Rev Mol Cell Biol *12*, 349-361. 10.1038/nrm3118.

Brinegar, A.E., Xia, Z., Loehr, J.A., Li, W., Rodney, G.G., and Cooper, T.A. (2017). Extensive alternative splicing transitions during postnatal skeletal muscle development are required for calcium handling functions. Elife *6*. 10.7554/eLife.27192.

Chen, B., You, W., Wang, Y., and Shan, T. (2020). The regulatory role of Myomaker and Myomixer-Myomerger-Minion in muscle development and regeneration. Cell Mol Life Sci *77*, 1551-1569. 10.1007/s00018-019-03341-9.

Chen, J.C., Mortimer, J., Marley, J., and Goldhamer, D.J. (2005). MyoD-cre transgenic mice: a model for conditional mutagenesis and lineage tracing of skeletal muscle. Genesis *41*, 116-121. 10.1002/gene.20104.

Cheng, Y., Luo, C., Wu, W., Xie, Z., Fu, X., and Feng, Y. (2016). Liver-Specific Deletion of SRSF2 Caused Acute Liver Failure and Early Death in Mice. Mol Cell Biol *36*, 1628-1638. 10.1128/MCB.01071-15.

Choi, S., Ferrari, G., and Tedesco, F.S. (2020). Cellular dynamics of myogenic cell migration: molecular mechanisms and implications for skeletal muscle cell therapies. EMBO Mol Med *12*, e12357. 10.15252/emmm.202012357.

Csapo, R., Gumpenberger, M., and Wessner, B. (2020). Skeletal Muscle Extracellular Matrix - What Do We Know About Its Composition, Regulation, and Physiological Roles? A Narrative Review. Front Physiol *11*, 253. 10.3389/fphys.2020.00253.

D'Cruz, R., Plant, P.J., Pablo, L.A., Lin, S., Chackowicz, J., Correa, J., Bain, J., and Batt, J. (2016). PDLIM7 is a novel target of the ubiquitin ligase Nedd4-1 in skeletal muscle. Biochem J *473*, 267-276. 10.1042/BJ20150222.

D'Urso, M., and Kurniawan, N.A. (2020). Mechanical and Physical Regulation of Fibroblast-Myofibroblast Transition: From Cellular Mechanoresponse to Tissue Pathology. Front Bioeng Biotechnol *8*, 609653. 10.3389/fbioe.2020.609653.

Du, R., Huang, C., Liu, K., Li, X., and Dong, Z. (2021). Targeting AURKA in Cancer: molecular mechanisms and opportunities for Cancer therapy. Mol Cancer *20*, 15. 10.1186/s12943-020-01305-3.

Fugier, C., Klein, A.F., Hammer, C., Vassilopoulos, S., Ivarsson, Y., Toussaint, A., Tosch, V., Vignaud, A., Ferry, A., Messaddeq, N., et al. (2011). Misregulated alternative splicing of BIN1 is associated with T tubule alterations and muscle weakness in myotonic dystrophy. Nat Med *17*, 720-725. 10.1038/nm.2374.

Golden, E., Rashwan, R., Woodward, E.A., Sgro, A., Wang, E., Sorolla, A., Waryah, C., Tie, W.J., Cuyas, E., Ratajska, M., et al. (2021). The oncogene AAMDC links PI3K-AKT-mTOR signaling with metabolic reprograming in estrogen receptor-positive breast cancer. Nat Commun *12*, 1920. 10.1038/s41467-021-22101-7.

Guo, R., You, X., Meng, K., Sha, R., Wang, Z., Yuan, N., Peng, Q., Li, Z., Xie, Z., Chen, R., and Feng, Y. (2022). Single-Cell RNA Sequencing Reveals Heterogeneity of Myf5-Derived Cells and Altered Myogenic Fate in the Absence of SRSF2. Adv Sci (Weinh) *9*, e2105775. 10.1002/advs.202105775.

Ji, X., Zhou, Y., Pandit, S., Huang, J., Li, H., Lin, C.Y., Xiao, R., Burge, C.B., and Fu, X.D. (2013). SR proteins collaborate with 7SK and promoter-associated nascent RNA to release paused polymerase. Cell *153*, 855-868. 10.1016/j.cell.2013.04.028.

Jirka, C., Pak, J.H., Grosgogeat, C.A., Marchetii, M.M., and Gupta, V.A. (2019). Dysregulation of NRAP degradation by KLHL41 contributes to pathophysiology in nemaline myopathy. Hum Mol Genet *28*, 2549-2560. 10.1093/hmg/ddz078.

Lappalainen, P., Kotila, T., Jegou, A., and Romet-Lemonne, G. (2022). Biochemical and mechanical regulation of actin dynamics. Nat Rev Mol Cell Biol *23*, 836-852. 10.1038/s41580-022-00508-4.

Lodka, D., Pahuja, A., Geers-Knorr, C., Scheibe, R.J., Nowak, M., Hamati, J., Kohncke, C., Purfurst, B., Kanashova, T., Schmidt, S., et al. (2016). Muscle RING-finger 2 and 3 maintain striated-muscle structure and function. J Cachexia Sarcopenia Muscle *7*, 165-180. 10.1002/jcsm.12057.

Nalbandian, M., Zhao, M., Kato, H., Jonouchi, T., Nakajima-Koyama, M., Yamamoto, T., and Sakurai, H. (2022). Single-cell RNA-seq reveals heterogeneity in hiPSC-derived muscle progenitors and E2F family as a key regulator of proliferation. Life Sci Alliance *5*. 10.26508/lsa.202101312.

Namgoong, S., and Kim, N.H. (2018). Meiotic spindle formation in mammalian oocytes: implications for human infertility. Biol Reprod *98*, 153-161. 10.1093/biolre/iox145.

Nicot, A.S., Toussaint, A., Tosch, V., Kretz, C., Wallgren-Pettersson, C., Iwarsson, E., Kingston, H., Garnier, J.M., Biancalana, V., Oldfors, A., et al. (2007). Mutations in amphiphysin 2 (BIN1) disrupt interaction with dynamin 2 and cause autosomal recessive centronuclear myopathy. Nat Genet *39*, 1134-1139. 10.1038/ng2086.

Nowak, K.J., Ravenscroft, G., and Laing, N.G. (2013). Skeletal muscle alpha-actin diseases (actinopathies): pathology and mechanisms. Acta Neuropathol *125*, 19-32. 10.1007/s00401-012-1019-z.

Osses, N., Casar, J.C., and Brandan, E. (2009). Inhibition of extracellular matrix assembly induces the expression of osteogenic markers in skeletal muscle cells by a BMP-2 independent mechanism. BMC Cell Biol *10*, 73. 10.1186/1471-2121-10-73.

Pathak, P., Blech-Hermoni, Y., Subedi, K., Mpamugo, J., Obeng-Nyarko, C., Ohman, R., Molloy, I., Kates, M., Hale, J., Stauffer, S., et al. (2021). Myopathy associated LDB3 mutation causes Z-disc disassembly and protein aggregation through PKCalpha and TSC2-mTOR downregulation. Commun Biol *4*, 355. 10.1038/s42003-021-01864-1.

Prokic, I., Cowling, B.S., and Laporte, J. (2014). Amphiphysin 2 (BIN1) in physiology and diseases. J Mol Med (Berl) *92*, 453-463. 10.1007/s00109-014-1138-1.

Relaix, F., Montarras, D., Zaffran, S., Gayraud-Morel, B., Rocancourt, D., Tajbakhsh, S., Mansouri, A., Cumano, A., and Buckingham, M. (2006). Pax3 and Pax7 have distinct and overlapping functions in adult muscle progenitor cells. J Cell Biol *172*, 91-102. 10.1083/jcb.200508044.

Relaix, F., Rocancourt, D., Mansouri, A., and Buckingham, M. (2005). A Pax3/Pax7-dependent population of skeletal muscle progenitor cells. Nature *435*, 948-953. 10.1038/nature03594.

Rodriguez-Outeirino, L., Hernandez-Torres, F., Ramirez-de Acuna, F., Matias-Valiente, L., Sanchez-Fernandez, C., Franco, D., and Aranega, A.E. (2021). Muscle Satellite Cell Heterogeneity: Does Embryonic Origin Matter? Front Cell Dev Biol *9*, 750534. 10.3389/fcell.2021.750534.

Schiaffino, S., Rossi, A.C., Smerdu, V., Leinwand, L.A., and Reggiani, C. (2015). Developmental myosins: expression patterns and functional significance. Skelet Muscle *5*, 22. 10.1186/s13395-015-0046-6.

Tajbakhsh, S., Rocancourt, D., and Buckingham, M. (1996). Muscle progenitor cells failing to respond to positional cues adopt non-myogenic fates in myf-5 null mice. Nature *384*, 266-270. 10.1038/384266a0.

Tajbakhsh, S., Rocancourt, D., Cossu, G., and Buckingham, M. (1997). Redefining the genetic hierarchies controlling skeletal myogenesis: Pax-3 and Myf-5 act upstream of MyoD. Cell *89*, 127-138. 10.1016/s0092-8674(00)80189-0.

Thomas, J.D., Oliveira, R., Sznajder, L.J., and Swanson, M.S. (2018). Myotonic Dystrophy and Developmental Regulation of RNA Processing. Compr Physiol *8*, 509-553. 10.1002/cphy.c170002.

Tong, M., Mukai, R., Mareedu, S., Zhai, P., Oka, S.I., Huang, C.Y., Hsu, C.P., Yousufzai, F.A.K., Fritzky, L., Mizushima, W., et al. (2023). Distinct Roles of DRP1 in Conventional and Alternative Mitophagy in Obesity Cardiomyopathy. Circ Res *133*, 6-21. 10.1161/CIRCRESAHA.123.322512.

Trapnell, C., Cacchiarelli, D., Grimsby, J., Pokharel, P., Li, S., Morse, M., Lennon, N.J., Livak, K.J., Mikkelsen, T.S., and Rinn, J.L. (2014). The dynamics and regulators of cell fate decisions are revealed by pseudotemporal ordering of single cells. Nat Biotechnol *32*, 381-386. 10.1038/nbt.2859.

Xiao, L., Xian, H., Lee, K.Y., Xiao, B., Wang, H., Yu, F., Shen, H.M., and Liou, Y.C. (2015). Death-associated Protein 3 Regulates Mitochondrial-encoded Protein Synthesis and Mitochondrial Dynamics. J Biol Chem *290*, 24961-24974. 10.1074/jbc.M115.673343.

Yin, H., Price, F., and Rudnicki, M.A. (2013). Satellite cells and the muscle stem cell niche. Physiol Rev *93*, 23-67. 10.1152/physrev.00043.2011.

Yin, H., Zhao, J., He, H., Chen, Y., Wang, Y., Li, D., and Zhu, Q. (2020). Gga-miR-3525 Targets PDLIM3 through the MAPK Signaling Pathway to Regulate the Proliferation and Differentiation of Skeletal Muscle Satellite Cells. Int J Mol Sci *21*. 10.3390/ijms21155573.

Zammit, P.S., Golding, J.P., Nagata, Y., Hudon, V., Partridge, T.A., and Beauchamp, J.R. (2004). Muscle satellite cells adopt divergent fates: a mechanism for self-renewal? J Cell Biol *166*, 347-357. 10.1083/jcb.200312007.

Zhang, W., Liu, Y., and Zhang, H. (2021). Extracellular matrix: an important regulator of cell functions and skeletal muscle development. Cell Biosci *11*, 65. 10.1186/s13578-021-00579-4.

Zhou, X., Li, X., Cheng, Y., Wu, W., Xie, Z., Xi, Q., Han, J., Wu, G., Fang, J., and Feng, Y. (2014).

BCLAF1 and its splicing regulator SRSF10 regulate the tumorigenic potential of colon cancer cells. Nat Commun *5*, 4581. 10.1038/ncomms5581.